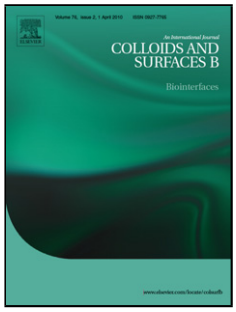

Title: PLLA/ZnO nanocomposites: dynamic surfaces to harness cell differentiation

Author: Sara Trujillo Erlantz Lizundia José Luis Vilas Manuel Salmeron-Sancheza

PII: S0927-7765(16)30264-8
DOI: http://dx.doi.org/doi:10.1016/j.colsurfb.2016.04.007
Reference: COLSUB 7800

To appear in: *Colloids and Surfaces B: Biointerfaces*

Received date: 1-12-2015
Revised date: 15-3-2016
Accepted date: 4-4-2016

Please cite this article as: Sara Trujillo, Erlantz Lizundia, José Luis Vilas, Manuel Salmeron-Sancheza, PLLA/ZnO nanocomposites: dynamic surfaces to harness cell differentiation, Colloids and Surfaces B: Biointerfaces http://dx.doi.org/10.1016/j.colsurfb.2016.04.007

Word count: 5513

Tables: 1

Figures: 6

Suplementary figures: 4

Full Paper

PLLA/ZnO nanocomposites: dynamic surfaces to harness cell differentiation

Sara Trujillo[a#], Erlantz Lizundia[b#], José Luis Vilas[b,c] and Manuel Salmeron-Sanchez[a*]

[a] Division of Biomedical Engineering, School of Engineering, University of Glasgow G12 8LT Glasgow, United Kingdom.

[b] Macromolecular Chemistry Research Group. Department of Physical Chemistry. Faculty of Science and Technology. University of the Basque Country (UPV/EHU), Spain.

[c] Basque Center for Materials, Applications and Nanostructures (BCMaterials), Parque Tecnológico de Bizkaia, Ed. 500, Derio 48160, Spain.

# These two authors contributed equally to this work

*Corresponding author: Manuel Salmeron-Sanchez; Manuel.Salmeron-Sanchez@glasgow.ac.uk

Graphical abstract

PLLA degradation
and NPs exposure

ZnO NPs loaded-PLLA

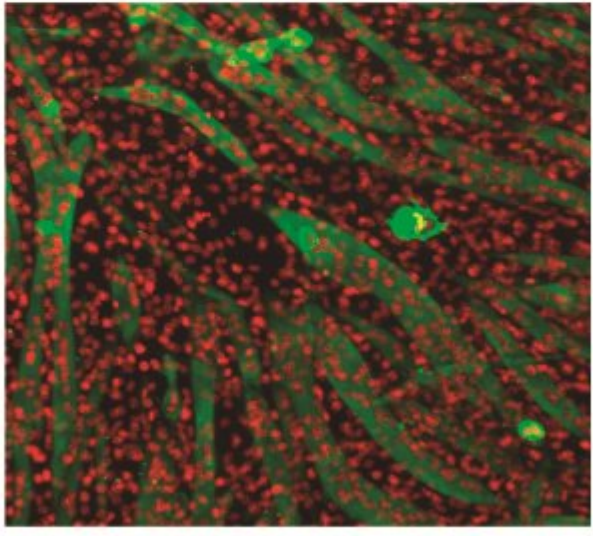

Myodifferentiation

Highlights

- Biodegradable poly(L-lactide) matrix loaded with ZnO nanorods.
- Dynamic presentation of nanorods triggered by PLLA degradation.
- Changes in surface properties as a function of time control cell behaviour.
- Nanorods exposure promotes cell differentiation.

Keywords: PLLA, ZnO nanoparticle, C2C12 myoblast, nanocomposite, cell differentiation

Abstract

This work investigates the effect of the sequential availability of ZnO nanoparticles, (nanorods of ~ 20 nm) loaded within a degradable poly(lactic acid) (PLLA) matrix, in cell differentiation. The system constitutes a dynamic surface, in which nanoparticles are exposed as the polymer matrix degrades. ZnO nanoparticles were loaded into PLLA and the system was measured at different time points to characterise the time evolution of the physicochemical properties, including wettability and thermal properties. The micro and nanostructure were also investigated using AFM, SEM and TEM images. Cellular experiments with C2C12 myoblasts show that cell differentiation was significantly enhanced on ZnO nanoparticles – loaded PLLA, as the polymer degrades and the availability of nanoparticles become more apparent, whereas the release of zinc within the culture medium was negligible. Our results suggest PLLA/ZnO nanocomposites can be used as a dynamic system where nanoparticles are exposed during degradation, activating the material surface and driving cell differentiation.

1. Introduction

Poly(lactic acid) (PLLA) is a semicrystalline, [1] aliphatic polyester extensively used in tissue engineering for many reasons; it is a biodegradable thermoplastic that presents biocompatibility, very low toxicity and can be shaped into different forms. [2-5] Numerous authors have modified PLLA to improve its characteristics for scaffolding in tissue engineering; to this purpose, PLLA has been blended with other polymers or inorganic materials to create composites. Different inorganic materials have been used such as hydroxyapatite (HAp), [6, 7] carbon nanotubes (CNTs), [8-10] bioactive glasses [11, 12] or metallic nanoparticles (NPs) [13, 14].

NPs are promising aspirants to be used in nanomedicine; because of their small size they can work at the scale of biomolecules, allowing more specific interactions with cells. [15, 16] Particularly, NP–loaded systems enhance cellular processes *in vitro*. For example, PLLA/iron oxide nanocomposites have shown neurite extension in electrospun microfibers, Cai et al. showed that PLLA/Fe_3O_4 composites enhanced osteogenic differentiation [17] and in a similar way Dong et al. showed enhanced osteogenic differentiation with PLLA/dicalcium silicate fibres. [18]

In this context, ZnO NPs have attracted attention as antimicrobials [19, 20] and UV blockers, [21] among others. Moreover, zinc is an essential element for cells, which acts as an intracellular secondary messenger in different cellular processes, [22, 23] in particular, the lack of zinc can inhibit myoblast differentiation. [24, 25] More recently has been shown that zinc promotes myoblast proliferation and differentiation via the activation of the ERK/Akt signalling cascade. [26] ZnO NPs have demonstrated their preferential ability to kill high proliferative cells, like cancer cells, versus normal cells. [19, 27] In addition, the oxidative stress properties of ZnO NPs have been also tested; [28] ZnO NPs can be sequestered by autophagy and this internalization could generate reactive oxygen species (ROS) intracellularly. [29] The effect of

surfaces containing ZnO in cell behaviour has been investigated previously. Osteoblast adhesion has been shown to be elevated on ZnO surfaces with high roughness (~ 30 nm), prepared by compression of ZnO NPs. [30] ZnO nanorod-coated surfaces were shown to be cytotoxic to macrophages regardless of the underlying topography [31] and has been reported to be cytotoxic to neuroblastoma cells and vascular endothelial cells with similar Zn concentrations (~150 μM). [32, 33]A recent study showed that electrospun nanofibres of ZnO/TiO_2 NPs resulted in increased cell proliferation of C2C12 myoblasts, although cell differentiation was not addressed. [13]

In this work, ZnO NPs have been loaded into a PLLA matrix to promote cell differentiation. We used C2C12 myoblasts because of their differentiation potential towards osteogenic and myogenic lineages [34] and the suggested role of zinc in myoblast differentiation. [26] We show that NPs are not released into the culture medium at the timescale we work with, but they are available on the material surface as time progresses. These changes in surface physicochemical properties, while the presentation of the nanoparticle is taking place, is enough to trigger higher cellular processes, such as cell differentiation.

2. Experimental section

2.1. Sample preparation

Samples were prepared by solvent-precipitation followed by compression moulding. First, ZnO NPs (L´Urederra technological centre (ES), rod-shaped structure with 43 ± 24 nm dimensions in length as measured in a previous work) [35] were homogeneously suspended in chloroform (LabScan, ≥ 99.8%) via mild-sonication (20% output for 5 min, Vibra-Cell™ CV 334) and added to previously dissolved PLLA (Purac Biochem (NL), number-average molecular weight (M_n) of 100 kDa and polydispersity index (M_w/M_n) of 1.85), at a concentration of 1wt. %. Another sonication step during 10 min was applied to disperse the NPs before precipitation in methanol (Panreac (ES), ≥ 99.5%) excess. This method ensures a

homogeneous distribution of NPs within the polymer matrix. After drying the resulting materials for 72 h at 70 ºC in a vacuum-oven, films with a thickness of ~150 µm were fabricated in a hydraulic hot press by compression moulding at 190 ºC for 4 min under a pressure of 150 MPa. Subsequently, films were water quenched to avoid the development of large crystalline fractions.

2.2. Transmission electron microscopy (TEM)

ZnO NPs were analyzed under transmission electron microscopy (TEM). A droplet of diluted suspension (0.1% (w/w)) in chloroform was deposited on carbon-coated grids. TEM was carried out using a Philips CM120 Biofilter apparatus with STEM module at an acceleration voltage of 120 kV. Images were acquired with a Morada digital camera.

2.3. Field Emission Scanning Electron Microscopy (FESEM)

Nanoparticle dispersion studies within the polymeric matrix were performed in a Hitachi S-4800 field emission scanning electron microscope (FE-SEM) at an acceleration voltage of 5 kV. Cryogenically fractured surfaces were cobalt-coated in a Quorum Q150T ES turbo-pumped sputter coater (5 nm thick coating).

2.4. *Atomic force microscopy (AFM)*

Surface topology features were analyzed using a Dimension ICON atomic force microscope (AFM) from Bruker (Bruker Corporation, Coventry, UK). Experiments were carried out in tapping mode with an integrated silicon tip/cantilever. Surface roughness of specimens was quantified by both root mean square roughness (R_q) and mean roughness (R_a) parameters as follows:

$$R_q = \sqrt{\frac{\sum_{i=1}^{N}(Z_i - Z_{ave})^2}{N}} \quad (1)$$

$$R_a = \frac{\sum_{i=1}^{N}|Z_i - Z_{cp}|}{N} \quad (2)$$

Where Z_{ave} is the average Z value within the analyzed area, N is the number of points, Z_i is the current Z value and Z_{cp} is the Z value of the centre plane.

Mechanical properties of the films were obtained by indentation tests. Samples were probed using a JPK NanoWizard III Atomic Force Microscope (JPK instruments AG, Berlin (DE)) with a pyramidal-shaped silica tip/cantilever (ACTA probes, AppNano, CA, US). The probe was calibrated using the thermal fluctuation method obtaining a nominal spring constant of ~ 40 N/m. Force indentation curves were obtained using the force mapping mode over areas of 30 μm^2 (25 measurements per map, n > 100 curves). A force of 4 μN with a constant speed (2.5 μm/s) was applied to obtain approximately 50 nm indentation. Each indentation curve was analysed using the Hertzian model for a pyramidal tip (JPK software, spm-4.3.50) from which the Young's modulus values were calculated. The Poisson's ratio for incompressible materials was used ($\nu = 0.5$).

2.5. Wide angle X-ray diffraction (WAXD)

Wide angle X-ray diffraction (WAXD) was conducted to elucidate the crystalline structure of ZnO nanoparticles. X-ray powder diffraction patterns were collected in a PHILIPS X'PERT PRO automatic diffractometer in theta-theta configuration, secondary monochromator with Cu-Kα radiation (λ = 1.5418 Å) and a PIXcel solid state detector. The sample was mounted on a zero background silicon wafer fixed in a generic sample holder. Data were collected from 20 to 75° 2θ (step size = 0.026) at room temperature (RT).

2.6. Hydrolytic degradation

150 μm thick square-shaped specimens were hydrolytically degraded at 37 ºC in a Phosphate Buffer solution (PBS, Sigma (UK); pH=7.4) and were removed after different periods of

time. The pH evolution of the medium was monitored using a 691 pH Meter (Metrohm). Water absorption (WA) and remaining weight (RW) values were determined according to:

$$WA = \frac{W_W - W_d}{W_d} \cdot 100 \quad (3)$$

$$RW = \frac{W_d}{W_0} \cdot 100 \quad (4)$$

Where W_w, W_d and W_0 are wet (obtained immediately after wiping films with a filter paper), dry (obtained after vacuum-drying at 60 ºC for 24 h) and initial weights, respectively.

2.7. Differential scanning calorimetry (DSC)

The thermal behaviour of hydrolytically degraded samples was determined using a Mettler Toledo DSC 822e calorimeter under nitrogen atmosphere (30 mL/min). Before thermal characterization, DSC temperature and enthalpy calibrations were performed using indium as standard (with an instrument accuracy of ±0.2 K). Samples were sealed in an aluminium pan and heated from -20 ºC to 200 ºC at a rate of 10 ºC/min to determine the thermal transitions (T_g, ΔH_{cc} and ΔH_m). The crystalline fraction X_c (%) attributable to the PLLA crystallization during the corresponding heat treatment was determined as follows: [36]

$$X_c(\%) = \frac{\Delta H_f - \Delta H_c}{\Delta H_f^0 \cdot W_m} \cdot 100 \quad (5)$$

where ΔH_f and ΔH_c are respectively the enthalpy of fusion and cold crystallization of the samples determined on the DSC and W_m is the PLLA matrix weight fraction in the composite sample. ΔH_f^0 = 106 J/g was taken as the heat of fusion of an infinitely thick PLLA crystal. [37]

2.8. Flame atomic absorption spectroscopy (FAAS)

Zinc concentration in the degradation medium was determined in a Perkin Elmer Analyst 800 flame atomic absorption spectrometer by FAAS using an oxidizing air/acetylene flame by measuring the absorbance at 213.9 nm. The amount of expeled Zn was calculated by

interpolation of the obtained absorbance values during the calibration curves (a standard Zn solution was employed for the construction of calibration curves).

2.9. Surface Zeta-potential measurement

Zeta-potential measurements based on Fairbrother-Mastin algorithm, which takes into account the conductivity of the employed electrolyte,[38] were performed using a commercially available Electrokinetic Analyzer for Solid Surface Analysis: SurPASS from Anton Paar GmbH (AT). Surface zeta potential (ζ) was measured at RT and a maximum pressure of 200 mbar using a 0.001 mol·dm^{-3} KCl electrolyte.

2.10. Cell culture

Murine C2C12 myoblasts at passage 3 were maintained in growth medium (Dulbecco's modified Eagle's medium (DMEM 4.5 g/L glucose + L-pyruvate, Gibco, MA, US) supplemented with 20% Foetal Bovine Serum (FBS, Gibco) and 1% Penicillin/Streptomycin) until seeding. Prior seeding, samples were sterilized by sonication immersing them in ethanol for 30 min. Glass coverslips were UV treated for 30 min.

2.11. Cell adhesion assay

Cell adhesion assay was carried out seeding C2C12 cells at 5000 cells/cm^2 in serum-free medium for 3 h (37 °C, 5% CO_2), in order to direct the adhesion to the protein coating. Protein coating was performed by adsorption of fibronectin (R&D Systems (UK), 20 µg/mL) for 1h at RT and then washing them twice with Dulbecco's Phosphate Buffered Saline (DPBS, Gibco). After 3 h of culture cells were fixed with 4% formaldehyde for 1 h at 4 °C and maintained in DPBS until further analysis. Glass coverslips coated with fibronectin (20 µg/mL, 1 h at RT) were used as controls.

2.12. Vinculin immunostaining

Samples were incubated in permeabilising buffer (0.5% Triton X-100 (Sigma, UK) in 20 mM HEPES buffer (Sigma) supplemented with 0.3 M sucrose, 50 mM NaCl (Sigma) and 3 mM $MgCl_2$ (Scharlab, ES)) for 5 min, and subsequently blocked in 1% bovine serum albumin (BSA, Gibco) for 1 h at RT. The primary monoclonal antibody hVIN-1 (Sigma) against vinculin was incubated for 1 h at RT (dilution 1:400) and washed three times in DPBS + 0.5% tween 20. Then, the secondary antibody Cy3 antimouse (Jackson Immunoresearch, US, dilution 1:200) was added with Phalloidin (Invitrogen (UK)), Dilution 1:300) to stain the actin cytoskeleton and were incubated for 1 h at RT. The secondary antibody was washed three times in DPBS + 0.5% Tween 20; finally, samples were mounted using mounting medium with DAPI (Vectashield-DAPI, Vector laboratories, US).

2.13. Viability test

Viability tests were performed seeding C2C12 cells at a density of 5000 cells/cm^2 in growth medium for 24 h, 3 d and 7 d. A mammalian LIVE/DEAD® assay (Invitrogen) was carried out at each selected time following the recommendations of the manufacturer. Briefly, samples were washed with DPBS and incubated with 4 µM of Ethidium homodimer-1 and 2 µM of calcein-AM for 30 min at 37 °C in darkness conditions. Finally, samples were mounted with mounting medium without DAPI (Vectashield) and different images were taken for quantification. Glass coverslips were used as controls.

2.14. Differentiation assay

Differentiation assay was assessed seeding C2C12 cells at 20000 cells/cm^2 in differentiation medium (Dulbecco's modified Eagle's medium (DMEM 4.5 g/L glucose + L-pyruvate) supplemented with 1% ITS-X (Insulin-transferrin-selenium-ethanolamine, Gibco) for 4 days, changing the medium the second day of culture. At the fourth day cells were fixed with 70% ethanol, 37% formaldehyde and glacial acetic acid at 10:1: 0.5 (V/V/V) ratio for 1 h at 4 °C, and subsequently stained for sarcomeric myosin. Prior to the seeding, samples were coated

with 10 µg/mL of fibronectin to facilitate cell attachment. Glass coverslips coated with both collagen (1 mg/mL, 1 h at RT) and then fibronectin (10 µg/mL, 1 h at RT) were used as positive controls.

2.15. Sarcomeric myosin immunostaining

Previous fixed cells were washed twice with DPBS. After washing, samples were blocked with blocking buffer (5% Goat Serum in DPBS) for 1 h at RT. The primary antibody anti-sarcomeric myosin (MF-20, Developmental Studies Hybridoma Bank, US) was used at a dilution 1:200 in blocking buffer for 1 h at RT. Then, samples were washed three times with DPBS + 0.5% tween 20 and blocked again with blocking buffer for 10 min at RT. After blocking, samples were washed twice with DPBS + 0.5% tween 20 and the secondary antibody rabbit anti-mouse Cy3 (Jackson Immunoresearch) was added at a dilution 1:250 in blocking buffer for 1 h at RT in darkness conditions. Finally, samples were washed three times with DPBS + 0.5% tween 20 and mounted with mounting medium (Vectashield-DAPI).

2.16. Proliferation assay

Myoblasts C2C12 were seeded (5000 cells/cm^2) on PLLA and PLLA/ZnO nanocomposites for two weeks using growth medium. The measurement of cell density was carried out through an AlamarBlue® (BioRad, UK) assay following manufaturer's recommendations. Briefly, 10% of AlamarBlue® was added at each time point to the culture medium for 3 h and then, the reduced product was measured by fluorescence in a plate reader at Ex/Em 560/590 nm with a manual gain of 72. A calibration curve was also assessed in order to correlate fluorescence intensity with cell density.

2.17. Image analysis

Cell adhesion assay images were analysed from the fluorescence images taken with a Zeiss Observer Z.1 microscope (Carl Zeiss, DE). Three different channels were acquired: blue for DAPI, green for phalloidin (actin cytoskeleton) and red for Cy3 (vinculin). Vinculin images were uploaded to the Focal Adhesion Analysis Server [39] using the actin cytoskeleton as cell mask. The images of binarized focal adhesions were measured using the Analyze particles tool in ImageJ (ImageJ 1.5b, National Institutes of Health (NIH)). Phalloidin images were used as well to study the morphology of cells (n > 50 cells).

Images from the LIVE/DEAD® assay were taken in order to count the number of live and dead cells. Two channels were acquired: green for calcein-AM (live cells) and red for Ethidium homodimer-1 (dead cells). The percentage of viable cells was calculated as the number of live cells per total number of cells.

The differentiation assay was analysed from the fluorescence images taken. Two different channels were acquired: blue for DAPI (nuclei) and red for Cy3 (sarcomeric myosin). DAPI images were counted using Find Maxima process (ImageJ) and an image of dots was outlined for each nucleus counted. Sarcomeric myosin binarized images were counted and multiplied by binarized nuclei images, so only nuclei under myotubes (assigned to differentiated cells) were counted. The differentiation percentage was calculated as differentiated cells per total number of cells.

2.18. Fibronectin adsorption quantification on films

Fibronectin (FN, from human plasma, R&D Systems, UK) was adsorbed onto PLLA or PLLA/ZnO from a solution of 20 µg/mL. The adsorption was carried out for 1 h (complete saturation) at RT using samples of 10 mm diameter. After that, the supernatant was collected and the amount of protein was quantified using a Micro BCA Assay Kit (Thermo Scientific, UK) following manufacturer's instructions. Finally, the amount of FN adsorbed was obtained

as the difference between the initial amount and the measured in the supernatant. Glass coverslips were used as controls.

2.19. Enzyme-linked immunosorbent assay (ELISA)

ELISA was performed on PLLA and PLLA/ZnO coated with FN (20 µg/mL, 1 h at RT) using a primary monoclonal antibody HFN7.1 (Developmental Studies Hybridoma Bank, IA, US) and a HRP-Goat Anti-Mouse (Invitrogen, CA, US) secondary antibody, coupled with a horseradish peroxidase for colorimetric detection. Controls without FN coatings were used as blank for each material. Samples were washed with DPBS twice, transferred to multiwell plates and blocked with BSA 1% for 30 min at RT. After that, samples were incubated with the primary antibody (1 h, RT, dilution 1:330) and washed twice with DPBS + tween 20 0.05%. The secondary antibody was then added (1 h, RT, dilution 1:10000) in dark conditions and washed twice with DPBS + tween 20 0.05%. Samples were transferred to a new multiwell plate and the substrate reagent (colour reagents A and B from R&D Systems, MN, US) was added (20 min, RT) in dark conditions. After substrate incubation, the reaction was stopped with a stop solution (R&D Systems) and transferred to a 96-well plate to read the absorbance at 450 and 540 nm.

2.20. Statistical analysis

The statistical analysis was assessed using GraphPad Prism 6.01. All values are expressed as mean ± SD and the number of replicates are specified for each assay. Parametric (ANOVA or t-test for homoscedastic data) and non-parametric (Kruskal-Wallis test when heteroscedastic data) tests were used depending on the experiment.

3. Results and discussion

3.1. Morphological characterization

Transmission electron microscopy (TEM) was used to determine the morphology of the ZnO nanoparticles. TEM micrographs (**Figure 1a**) confirmed the nanometric rod-shaped structure of the NPs, with ~20 nm width and ~43 nm length (particle size-distribution determined from 10 TEM images). Additionally, wide angle X-ray diffraction pattern (Supporting Information, **Figure S1**) showed featured reflections of the hexagonal Wurtzite crystal system.

It is well established that the nanoparticle dispersion within the polymeric matrix plays a key role on the physical properties of the material, which in turn influences the resulting cell/material interaction. [8, 9] In this sense, both bulk and surface nanoparticle dispersion were evaluated by field emision scanning electron microscopy (FE-SEM) and atomic force microscopy (AFM) respectively. **Figure 1b** shows a representative FE-SEM micrograph of cryogenically fractured PLLA/ZnO 1 wt.% nanocomposite surface, where nanoparticles can be observed homogeneously distributed throughout the polymer matrix. **Figure 2a** and **2d** display the surface features of initial non-degraded neat PLLA and PLLA/ZnO film respectively. R_q and R_a surface roughness parameters, which quantitatively determine the average vertical deviation of the surface profile from the center plane, [40] are included. Images reveal that surface topology is slightly modified by ZnO NPs whereas the neat polymer shows a corrugated surface, nanocomposites present a flat surface with prominent ZnO nanoparticles. However, similar values of surface roughness were measured on both PLLA and the nanocomposite, which suggests that the overall topography of the surface does not change by the presence of the NPs, as previously reported for other PLLA based nanocomposites. [9]

3.2. Hydrolytic degradation of films at 37 °C

PLLA/ZnO nanocomposites were hydrolytically degraded at 37 ºC for 15 days. The extent of hydrolytic degradation was followed by differential scanning calorimetry (DSC, **Figure S2**),

pH changes, water absorption (WA) and remaining weight (RW) measurements (**Table 1**). After 8 days, the crystallinity (X_c) of neat PLLA specimens slightly increases from 12.1% to 19.3% whereas the X_c increase is more noticeable on the nanocomposites (from 13.2% to 47.3%) as degradation proceeds, likely due to the presence of nanoparticles that act as catalytic nuclei to prompt the hydrolytic degradation of the PLLA polymer. Moreover, a decrease was observed in the cold crystallization temperature (T_{cc}) in both specimens. This effect is ascribed to the progressive chain-shortening via random-scission of ester linkages, [41] which increases the chain mobility and boosts the development of highly-ordered crystalline phases. [42]

The pH evolution of the medium gives further insights about the hydrolytic degradation of specimens; a pH decrease would indicate a release of acidic by-products from the material to the medium. The fact that pH, together with remaining weight (RW) and water absorption (WA), remains almost stable after 8 days denotes the absence of large amounts of carboxylic end-groups arising from the hydrolytic degradation of PLLA. After 15 days, **Table 1** shows more changes that suggest a higher progress of degradation on the PLLA/ZnO system in comparison to neat PLLA. This result is in accordance with recent studies that show ZnO nanoparticles as accelerators of the hydrolytic degradation of PLLA in water at temperatures below T_g. [43]

Figure 2 depicts AFM height and phase images of both neat PLLA and ZnO-loaded PLLA upon hydrolytic degradation at 37 ºC. The corrugated surface of PLLA becomes smoother as time goes by, quantified by the decrease in the overall R_q from 43.2 nm to 21.5 nm (**Figure 2** and **Figure 3b**). However, degradation of PLLA/ZnO involves significant local topological changes on the surface, with the formation of nanoscale pits throughout the sample and R_q increasing from 32.1 nm to 132 nm after 15 days. This behaviour is related to the degradation

of PLLA surrounding ZnO nanoparticles. The phase image suggests that NPs remain on the surface after 15 days, but are not covered by a polymer layer (**Figure 2**). Note that long-term degradation of the system could lead to a complete ejection of the NPs, which can be internalized by cells, generating ROS and inducing cytotoxicity. [29] However, the degradation of PLLA can be tuned to prevent these unwanted effects in a broad time window. [44-46] This is interesting not only to avoid a possible long-term cytotoxicity but also to control when the NPs are exposed on the surface of PLLA.

We have also determined the amount of zinc released into the supernatant as a function of time by flame atomic absorption spectroscopy (FAAS), a technique especially suitable for the accurate quantification of heavy metals. [47, 48] Results show that films release an average zinc concentration of 5 ng/mm^2 after 8 days and 6.5 ng/mm^2 (~ 3 μM) after 15 days (**Figure 3**). Those results are in accordance with AFM morphological characterizations where the development of craters surrounding ZnO nanoparticles are observed, with most of the particles still on the surface (**Figure 2**). The reported cytotoxic zinc concentration, using different cell types, in culture is 150 μM, [32] which suggests that the amount of zinc released in our system is slow enough to not create adverse cellular effects due to the presence of zinc. In the light of obtained FAAS results, together with data shown in **Table 1** and AFM images, a model depicting ZnO release to the medium is shown in **Figure 3,** where the cross-section of PLLA/ZnO nanocomposite is shown in grey and ZnO nanoparticles are depicted as thick blue bars. When the hydrolytic degradation of PLLA starts (white line) only a small fraction of NPs on the surface is not covered by PLLA as confirmed by FE-SEM and AFM (**Figure 1 and Figure 2**), with similar measurements of roughness for both PLLA and PLLA/ZnO (**Figure 3b**). As degradation of PLLA proceeds, NPs are continuously exposed on the surface

(after ~ 8 days) and finally only a few of them are released into the medium after 15 days of hydrolytic degradation (**Figure 3b**, small amounts of zinc detected by FAAS).

3.3. Cell culture studies

3.3.1. Biocompatibility, cell adhesion and morphology

We first wanted to disregard the potential cytotoxicity of the system – some authors have reported that ZnO might be cytotoxic under certain conditions – [31-33] using a LIVE/DEAD® assay. To do so, C2C12 were seeded onto the surfaces with growth medium for 1 week. **Figure 4a** shows the LIVE/DEAD® staining at 1, 3 and 7 days of culture for PLLA/ZnO. Viability of C2C12 myoblasts on the PLLA/ZnO nanocomposite was ~ 99% after 7 days, similar to the negative control (**Figure 4b**). In this experiment cells are in direct contact with the surface of the material, which suggests the lack of release of any cytotoxic compound. Taking into account the data obtained by FAAS, in which a total zinc release of 5 ng/mm^2 at 8 days was observed, it is reasonable to think that the small release detected was not cytotoxic. These results are in accordance with other studies that estimated the minimum ZnO NP concentration that causes the inflammation response in endothelial cells to be 10 µg/mL (~ 150 µM), [33] which is 50 times the concentration of Zn measured in our system. From the images, we also quantified cell density (**Figure 4c**) that increased linearly as a function of time. The number of cells was higher on the nanocomposite, but not significant.

Afterwards, we investigated initial cell adhesion and spreading on the nanocomposites. Cells interact with synthetic surfaces through a layer of adsorbed proteins, on which cells adhere and spread before other cellular processes such as cell proliferation or differentiation occur.

We first studied the behaviour of FN on the material surfaces. We selected FN because it is one of the major constituents of the extracellular matrix and presents a promiscuous cell-

attachment sequence (the RGD sequence) that can be recognised by multiple integrins.[49] We quantified the amount of adsorbed FN and the conformation via the availability of RGD domains using a monoclonal antibody (HFN7.1) against the region between the 9th and 10th FN-type III repeating domains in which the RGD sequence resides. [50] **Figure 4d** shows the surface density of fibronectin (ng/cm^2) that was significantly higher on PLLA/ZnO than PLLA. **Figure 4e** shows higher availability of RGD on fibronectin adsorbed onto PLLA/ZnO. Normalisation of **Figure 4e,** using the amount of FN on the surface (**Figure 4f**), results in no differences between material systems. This is likely a consequence of the higher amount of protein initially adsorbed onto the PLLA/ZnO, as opposed to PLLA, rather than any differences in FN conformation.

Cell morphology after 3 h of culture was very similar, and cells presented a well-developed actin cytoskeleton with tension fibres (**Figure 4g**) typical of cells cultured on 2D rigid substrates [51] (stiffness measured via indentation with the AFM was 3.417 ± 1.037 GPa for PLLA and 3.027 ± 0.760 GPa for PLLA/ZnO, **Figure S3**). Cell shape descriptors were calculated and shown in **Figure 4h**. Cell area, perimeter, roundness and circularity were similar between cells adhered on PLLA, PLLA/ZnO or glass control meaning that cells were well spread. **Figure 5a** and **Figure S4** show focal adhesions after 3 h studied via vinculin immunostaining. Interestingly, cells on PLLA/ZnO developed a higher number of focal adhesions (FA) than on PLLA (total FA count per cell, **Figure 5c**) and the area of the FA was significantly higher in PLLA/ZnO than pure PLLA. In addition, the distribution of the FA area shows the presence of a higher number of mature focal adhesions on the nanocomposite than the bulk polymer, including FAs bigger than 3 μm^2 (**Figure 5b**). The presence of the higher number and larger FAs on the nanocomposite, compared to neat PLLA, correlates with the surface density of fibronectin measured and thus with the presence of a higher number of RGD domains available for cell interaction.

It is well known that surface charge influence protein adsorption.[52, 53] To study whether the initial amount of adsorbed fibronectin on PLLA/ZnO was due to differences in the initial superficial charges of the surfaces, we measured the Z-potential. However, similar values were obtained for both surfaces, -30.20 ± 0.75 mV - PLLA and -33.07 ± 3.65mV - PLLA/ZnO, which disregards the possible effect of surface charge on the higher protein adsorption measured on the nanocomposite.

3.3.2. Cell proliferation and differentiation

We then analysed the ability of C2C12 cells to proliferate and differentiate on the nanocomposites. **Figure 6d** shows the proliferation curve obtained by means of an AlamarBlue® assay using neat PLLA and the ZnO nanocomposites for two weeks. At day 1 and 4 the number of cells was the same between materials, although the PLLA/ZnO nanocomposite presented lower proliferation rate at this time of culture. After one week, the number of cells increased, with the highest number of cells on the nanocomposites. During this week a typical plateau was observed, suggesting that cells reached confluence; therefore, at day 10 the number of cells quantified was similar to day 7 and, after 2 weeks the number of cells started to decrease, due to cell death from contact inhibition processes. It is interesting to note that cells seeded onto PLLA reached confluence at day 4, while on PLLA/ZnO nanocomposites continued growing. Nevertheless, differences observed were not statistically significant, which suggests that the release of zinc ions at this time was not enough to enhance cell proliferation, as has been suggested to happen with zinc concentrations within 25-50 μM.[26]

Myoblast differentiation was assessed by staining for sarcomeric myosin that, together with multinucleated myotube formation, is characteristic of the differentiation process (**Figure 6b, e**). Four days is the standard time required for C2C12 *in vitro* differentiation studies with myogenic differentiation medium; after that time, the percentage of differentiation was

similar between PLLA and PLLA/ZnO (**Figure 6c**). Moreover, at this time the amount of zinc released from the system to the medium is low (**Figure 3c**) and the hydrolytic degradation occurred is not enough to expose the nanoparticles on the surface; therefore, the changes in roughness at this point are also negligible. However, after two weeks of culture, differentiation was up to 30% higher on the nanocomposite than on neat PLLA (note that this was done in standard medium with 20% FBS, i.e. no soluble cues added) (**Figure 6f**). As can be seen on **Figure 6e**, mature, multinucleated myotubes were formed on the nanocomposite with larger area and thickness (~ 40 μm^2 area and > 40 μm thickness). The calculated fusion index, the number of nuclei per myotube, was consequently higher on the nanocomposite with more than 40% of myotubes containing ≥ 6 nuclei, whereas 40% of cells on PLLA presented only one nucleus (no fusion) (**Figure 6g**). This different cellular behaviour between PLLA and PLLA/ZnO was enhanced as a function of time (i.e. 4 d versus 14 d), which is correlated to the degradation of the superficial layer of PLLA and the appearance of ZnO nanoparticles on the material surface.

The dynamic presence of NPs alters different parameters such as surface roughness and the release of Zn into the culture medium. Changes in roughness do not seem to be a trigger of C2C12 differentiation; for example, stiff and smooth surfaces were found to favour C2C12 differentiation.[54] In addition, organised topographical patterns do not influence C2C12 differentiation compared to flat ones. [55, 56] Conversely, the release of zinc into the culture medium, as PLLA degradation proceeds, is very low compared to the amounts needed to promote C2C12 differentiation (~ 3 μM in our system), which is further diluted due to the periodical changes of the medium during culture, compare to 25-50 μM. [26]

For cell differentiation to occur, cells have to leave the cell cycle and hence, stop proliferation. After 4 days, the combination of the differentiation medium and the surface of PLLA are the modulators of myoblast differentiation, as it has been shown previously,[57] i.e.

there is no evident effect of the nanoparticles in cell differentiation. However, by maintaining a growing cell population longer, they leave the cell cycle triggered by the stimuli coming from the material system, as more nanoparticles are available on the material surface as PLLA degrades. [41, 42] Note that in this case the degradation rate could be essential in order to see differences in the percentage of differentiation and this can be easily tuned in PLLA.[44, 45]

4. Conclusions

In this work, we have engineered and characterised ZnO nanoparticle–loaded PLLA degradable system, with nanoparticles homogeneously dispersed on the PLLA surface. The availability of ZnO particles during the degradation of PLLA induces the formation of nanopits, containing particles, on the surface. Based on the low amount of released Zn compared to the amount of Zn necessary to trigger C2C12 differentiation, as well as the AFM images, the initial similar Z-potential and Young's modulus measured, we concluded that the availability of the ZnO NPs, as PLLA degrades on the material surface, is the cue for cell differentiation. In standard conditions, C2C12 myoblasts differentiate within 4 days as long as the adequate stimuli is provided. Surprisingly, our results show that only when PLLA degradation starts, after ~ 15 days, is cell differentiation significantly enhanced, which is correlated with the presence of NPs on the material surface. The system can be further engineered to control the degradation rate of PLLA and subsequently the timescale at which NPs are available on the material surface, which provides different cues for cell growth versus differentiation. Further biological studies are necessary to determine how the presence of NPs on the surface trigger signalling pathways, leading to myogenesis.

Acknowledgements

MSS acknowledges support from ERC through HealInSynergy (306990). EL thanks the

University of the Basque Country (UPV/EHU) for a postdoctoral fellowship. ST acknowledges support from the University of Glasgow through their internal scholarship funding program. We gratefully acknowledge Corbion-Purac for the kind donation of PLLA.

5. References

[1] E. Lizundia, J.L. Vilas, L.M. León, Crystallization, structural relaxation and thermal degradation in Poly(l-lactide)/cellulose nanocrystal renewable nanocomposites, Carbohydrate Polymers, 123 (2015) 256-265.
[2] M. Jamshidian, E.A. Tehrany, M. Imran, M. Jacquot, S. Desobry, Poly-Lactic Acid: Production, Applications, Nanocomposites, and Release Studies, Comprehensive Reviews in Food Science and Food Safety, 9 (2010) 552-571.
[3] A. Södergård, M. Stolt, Industrial Production of High Molecular Weight Poly(Lactic Acid), Poly(Lactic Acid), John Wiley & Sons, Inc.2010, pp. 27-41.
[4] M. Martina, D.W. Hutmacher, Biodegradable polymers applied in tissue engineering research: a review, Polymer International, 56 (2007) 145-157.
[5] H.-H. Lee, U. Sang Shin, J.-H. Lee, H.-W. Kim, Biomedical nanocomposites of poly(lactic acid) and calcium phosphate hybridized with modified carbon nanotubes for hard tissue implants, Journal of Biomedical Materials Research Part B: Applied Biomaterials, 98B (2011) 246-254.
[6] J.B. Lee, H.N. Park, W.-K. Ko, M.S. Bae, D.N. Heo, D.H. Yang, I.K. Kwon, Poly(L-lactic acid)/Hydroxyapatite Nanocylinders as Nanofibrous Structure for Bone Tissue Engineering Scaffolds, Journal of Biomedical Nanotechnology, 9 (2013) 424-429.
[7] S. Eftekhari, I. El Sawi, Z.S. Bagheri, G. Turcotte, H. Bougherara, Fabrication and characterization of novel biomimetic PLLA/cellulose/hydroxyapatite nanocomposite for bone repair applications, Materials Science and Engineering: C, 39 (2014) 120-125.
[8] E. Lizundia, J.R. Sarasua, F. D'Angelo, A. Orlacchio, S. Martino, J.M. Kenny, I. Armentano, Biocompatible Poly(L-lactide)/MWCNT Nanocomposites: Morphological Characterization, Electrical Properties, and Stem Cell Interaction, Macromolecular Bioscience, 12 (2012) 870-881.
[9] M. Obarzanek-Fojt, Y. Elbs-Glatz, E. Lizundia, L. Diener, J.-R. Sarasua, A. Bruinink, From implantation to degradation — are poly (l-lactide)/multiwall carbon nanotube composite materials really cytocompatible?, Nanomedicine: Nanotechnology, Biology and Medicine, 10 (2014) 1041-1051.
[10] S. Sun, I. Titushkin, M. Cho, Regulation of mesenchymal stem cell adhesion and orientation in 3D collagen scaffold by electrical stimulus, Bioelectrochemistry, 69 (2006) 133-141.
[11] Z. Zhou, J. Zhou, Q. Yi, L. Liu, Y. Zhao, H. Nie, X. Liu, J. Zou, L. Chen, Biological evaluation of poly-l-lactic acid composite containing bioactive glass, Polym. Bull., 65 (2010) 411-423.
[12] E. Zeimaran, S. Pourshahrestani, I. Djordjevic, B. Pingguan-Murphy, N.A. Kadri, M.R. Towler, Bioactive glass reinforced elastomer composites for skeletal regeneration: A review, Materials Science and Engineering: C, 53 (2015) 175-188.
[13] T. Amna, M. Shamshi Hassan, M.-S. Khil, H.-K. Lee, I.H. Hwang, Electrospun nanofibers of ZnO-TiO2 hybrid: characterization and potential as an extracellular scaffold for supporting myoblasts, Surface and Interface Analysis, 46 (2014) 72-76.
[14] M. Murariu, A. Doumbia, L. Bonnaud, A.L. Dechief, Y. Paint, M. Ferreira, C. Campagne, E. Devaux, P. Dubois, High-Performance Polylactide/ZnO Nanocomposites Designed for Films and Fibers with Special End-Use Properties, Biomacromolecules, 12 (2011) 1762-1771.
[15] S.B. Lanone, J., Biomedical applications and potential health risks of nanomaterials: molecular mechanisms, Current Molecular Medicine, 6 (2006) 13.
[16] S.E. McNeil, Nanotechnology for the biologist, Journal of Leukocyte Biology, 78 (2005) 585-594.

[17] Q. Cai, Y. Shi, D. Shan, W. Jia, S. Duan, X. Deng, X. Yang, Osteogenic differentiation of MC3T3-E1 cells on poly(l-lactide)/Fe3O4 nanofibers with static magnetic field exposure, Materials Science and Engineering: C, 55 (2015) 166-173.
[18] S. Dong, J. Sun, Y. Li, J. Li, W. Cui, B. Li, Electrospun nanofibrous scaffolds of poly (l-lactic acid)-dicalcium silicate composite via ultrasonic-aging technique for bone regeneration, Materials Science and Engineering: C, 35 (2014) 426-433.
[19] M. Premanathan, K. Karthikeyan, K. Jeyasubramanian, G. Manivannan, Selective toxicity of ZnO nanoparticles toward Gram-positive bacteria and cancer cells by apoptosis through lipid peroxidation, Nanomedicine: Nanotechnology, Biology and Medicine, 7 (2011) 184-192.
[20] P. Kanmani, J.-W. Rhim, Properties and characterization of bionanocomposite films prepared with various biopolymers and ZnO nanoparticles, Carbohydrate Polymers, 106 (2014) 190-199.
[21] E. Lizundia, L. Ruiz-Rubio, J.L. Vilas, L.M. León, Poly(l-lactide)/zno nanocomposites as efficient UV-shielding coatings for packaging applications, Journal of Applied Polymer Science, (2015) n/a-n/a.
[22] A. Truong-Tran, J. Carter, R. Ruffin, P. Zalewski, The role of zinc in caspase activation and apoptotic cell death, Biometals, 14 (2001) 315-330.
[23] B.L. Vallee, K.H. Falchuk, The biochemical basis of zinc physiology, Physiological Reviews, 73 (1993) 79-118.
[24] L. Petrie, J.N. Buskin, J.K. Chesters, Zinc and the initiation of myoblast differentiation, The Journal of Nutritional Biochemistry, 7 (1996) 670-676.
[25] L. Petrie, J.K. Chesters, M. Franklin, Inhibition of myoblast differentiation by lack of zinc, Biochemical Journal, 276 (1991) 109-111.
[26] K. Ohashi, Y. Nagata, E. Wada, P.S. Zammit, M. Shiozuka, R. Matsuda, Zinc promotes proliferation and activation of myogenic cells via the PI3K/Akt and ERK signaling cascade, Experimental Cell Research, 333 (2015) 228-237.
[27] H. Cory, L. Janet, P. Alex, K.M. Reddy, C. Isaac, C. Andrew, F. Kevin, W. Denise, Preferential killing of cancer cells and activated human T cells using ZnO nanoparticles, Nanotechnology, 19 (2008) 295103.
[28] M. Pandurangan, M. Veerappan, D. Kim, Cytotoxicity of Zinc Oxide Nanoparticles on Antioxidant Enzyme Activities and mRNA Expression in the Cocultured C2C12 and 3T3-L1 Cells, Appl Biochem Biotechnol, 175 (2015) 1270-1280.
[29] T. Xia, M. Kovochich, M. Liong, L. Mädler, B. Gilbert, H. Shi, J.I. Yeh, J.I. Zink, A.E. Nel, Comparison of the Mechanism of Toxicity of Zinc Oxide and Cerium Oxide Nanoparticles Based on Dissolution and Oxidative Stress Properties, ACS Nano, 2 (2008) 2121-2134.
[30] G. Colon, B.C. Ward, T.J. Webster, Increased osteoblast and decreased Staphylococcus epidermidis functions on nanophase ZnO and TiO2, Journal of Biomedical Materials Research Part A, 78A (2006) 595-604.
[31] T.D. Zaveri, N.V. Dolgova, B.H. Chu, J. Lee, J. Wong, T.P. Lele, F. Ren, B.G. Keselowsky, Contributions of surface topography and cytotoxicity to the macrophage response to zinc oxide nanorods, Biomaterials, 31 (2010) 2999-3007.
[32] H.A. Jeng, J. Swanson, Toxicity of Metal Oxide Nanoparticles in Mammalian Cells, Journal of Environmental Science and Health, Part A, 41 (2006) 2699-2711.
[33] A. Gojova, B. Guo, R.S. Kota, J.C. Rutledge, I.M. Kennedy, A.I. Barakat, Induction of Inflammation in Vascular Endothelial Cells by Metal Oxide Nanoparticles: Effect of Particle Composition, Environmental Health Perspectives, 115 (2007) 403-409.

[34] S. Burattini, P. Ferri, M. Battistelli, R. Curci, F. Luchetti, E. Falcieri, C2C12 myoblasts as a model of skeletal muscle development: morpho-functional characterization, European Journal of Histochemistry, 48 (2004) 223-234.
[35] E. Lizundia, A. Urruchi, J.L. Vilas, L.M. León, Increased functional properties and thermal stability of flexible cellulose nanocrystal/ZnO films, Carbohydrate Polymers, 136 (2016) 250-258.
[36] J. del Río, A. Etxeberria, N. López-Rodríguez, E. Lizundia, J.R. Sarasua, A PALS Contribution to the Supramolecular Structure of Poly(l-lactide), Macromolecules, 43 (2010) 4698-4707.
[37] J.-R. Sarasua, R.E. Prud'homme, M. Wisniewski, A. Le Borgne, N. Spassky, Crystallization and Melting Behavior of Polylactides, Macromolecules, 31 (1998) 3895-3905.
[38] F. F., M. H., Studies in electro-endosmosis, J. Chem. Soc., (1924) 2319-2330.
[39] M. Berginski, S. Gomez, The Focal Adhesion Analysis Server: a web tool for analyzing focal adhesion dynamics [version 1; referees: 2 approved], 2013.
[40] E. Lizundia, S. Petisco, J.-R. Sarasua, Phase-structure and mechanical properties of isothermally melt-and cold-crystallized poly (L-lactide), Journal of the Mechanical Behavior of Biomedical Materials, 17 (2013) 242-251.
[41] U. Edlund, A.C. Albertsson, Polyesters based on diacid monomers, Advanced Drug Delivery Reviews, 55 (2003) 585-609.
[42] Y. Gong, Q. Zhou, C. Gao, J. Shen, In vitro and in vivo degradability and cytocompatibility of poly(l-lactic acid) scaffold fabricated by a gelatin particle leaching method, Acta Biomaterialia, 3 (2007) 531-540.
[43] M. Qu, H. Tu, M. Amarante, Y.-Q. Song, S.S. Zhu, Zinc oxide nanoparticles catalyze rapid hydrolysis of poly(lactic acid) at low temperatures, Journal of Applied Polymer Science, 131 (2014) n/a-n/a.
[44] V. Arias, A. Höglund, K. Odelius, A.-C. Albertsson, Tuning the degradation profiles of poly (l-lactide)-based materials through miscibility, Biomacromolecules, 15 (2013) 391-402.
[45] C. Shasteen, Y. Choy, Controlling degradation rate of poly(lactic acid) for its biomedical applications, Biomed. Eng. Lett., 1 (2011) 163-167.
[46] S. Benali, S. Aouadi, A.-L. Dechief, M. Murariu, P. Dubois, Key factors for tuning hydrolytic degradation of polylactide/zinc oxide nanocomposites, Nanocomposites, 1 (2015) 51-61.
[47] J. Abulhassani, J.L. Manzoori, M. Amjadi, Hollow fiber based-liquid phase microextraction using ionic liquid solvent for preconcentration of lead and nickel from environmental and biological samples prior to determination by electrothermal atomic absorption spectrometry, Journal of Hazardous Materials, 176 (2010) 481-486.
[48] L. Zhang, X. Chang, Z. Li, Q. He, Selective solid-phase extraction using oxidized activated carbon modified with triethylenetetramine for preconcentration of metal ions, Journal of Molecular Structure, 964 (2010) 58-62.
[49] R. Pankov, K.M. Yamada, Fibronectin at a glance, Journal of Cell Science, 115 (2002) 3861-3863.
[50] B.G. Keselowsky, D.M. Collard, A.J. García, Surface chemistry modulates fibronectin conformation and directs integrin binding and specificity to control cell adhesion, Journal of Biomedical Materials Research Part A, 66A (2003) 247-259.
[51] C. Yang, M.W. Tibbitt, L. Basta, K.S. Anseth, Mechanical memory and dosing influence stem cell fate, Nat Mater, 13 (2014) 645-652.
[52] N. Faucheux, R. Schweiss, K. Lützow, C. Werner, T. Groth, Self-assembled monolayers with different terminating groups as model substrates for cell adhesion studies, Biomaterials, 25 (2004) 2721-2730.

[53] S. Roessler, R. Zimmermann, D. Scharnweber, C. Werner, H. Worch, Characterization of oxide layers on Ti6Al4V and titanium by streaming potential and streaming current measurements, Colloids and Surfaces B: Biointerfaces, 26 (2002) 387-395.
[54] X. Hu, S.-H. Park, E.S. Gil, X.-X. Xia, A.S. Weiss, D.L. Kaplan, The influence of elasticity and surface roughness on myogenic and osteogenic-differentiation of cells on silk-elastin biomaterials, Biomaterials, 32 (2011) 8979-8989.
[55] B.-B. José, L. Myriam, C. Hector, L. Andres Diaz, S.-S. Manuel, Robust fabrication of electrospun-like polymer mats to direct cell behaviour, Biofabrication, 6 (2014) 035009.
[56] J.L. Charest, A.J. García, W.P. King, Myoblast alignment and differentiation on cell culture substrates with microscale topography and model chemistries, Biomaterials, 28 (2007) 2202-2210.
[57] P. Rico, A. Rodrigo-Navarro, M. Salmerón-Sánchez, Borax-Loaded PLLA for Promotion of Myogenic Differentiation, Tissue Engineering Part A, (2015).

Captions to Figures

Figure 1. Morphological characterization of nanocomposites. (a) TEM image showing the structure of ZnO nanoparticles at a 230.000x magnification; **(b)** FE-SEM micrographs showing ZnO dispersion (e.g. arrows) in PLLA matrix.

Figure 2. AFM height and phase images showing surface features of neat PLLA and PLLA/ZnO nanocomposite. **(a)** The initially non-degraded matrices (0 d) and **(b, c)** 8-15 days degraded surfaces are shown; roughness values are highlighted. Scale bar: 2 μm.

Figure 3. Hydrolytic degradation mechanism. (a) Schematic representation of hydrolytic degradation in PLLA/ZnO nanocomposites, **(b)** Average roughness during hydrolytic degradation of PLLA and PLLA/ZnO nanocomposites and **(c)** representation of released mass of Zn per unit area measured by FAAS (± SD FAAS).

Figure 4. (a) C2C12 cells were grown for 7 days in growth medium onto PLLA/ZnO films and a LIVE/DEAD staining was assessed at 1, 3 and 7 days. Living cells are shown in green and dead cells in red. Scale bar: 50 μm. **(b)** Percentage of cell survival (mean ± SD) from the LIVE/DEAD staining and **(c)** cell density at 7 days (mean ± SD); **(d)** surface density after fibronectin adsorption for 1 h (ng/cm^2) (n = 3), (**e**) availability of the RGD sequence of the adsorbed fibronectin on the surfaces measured by ELISA (plotted as absorbance at 450 - absorbance at 540 nm) (n = 3), (**f**) normalized absorbance with the amount of fibronectin quantified in (**d**). **(g)** C2C12 actin cytoskeleton (green) and nuclei (blue) at 3 h culture (scale bar: 50 μm); **(h)** shape descriptors were quantified from 3 h culture (mean ± SD, n > 50), Roundness = 4[area]/π[major axis]^2, Circularity = 4π [area]/[perimeter]^2. Statistical differences in an unpaired t-test (*) p-value < 0.05, (***) p-value < 0.001. Glass coverslips were used as controls.

Figure 5. Focal adhesion analysis. (a) Representative binary images of the focal adhesions (FA) (scale bar: 25 μm), **(b)** Distribution of the focal adhesion areas (μm^2); **(c)** Focal adhesion count per cell analysed (n = 10, mean ± SD), **(d)** median of the focal adhesion areas (μm^2) (n = 10, mean ± SD)**, (e)** median of the focal adhesion size (μm) (n = 10, mean ± SD). Statistical differences using ANOVA test with a Tukey's *post hoc* test are shown as *** p-value < 0.001. Glass coverslips were used as controls.

Figure 6. Cell proliferation and cell differentiation. **(a)** Sketch showing the differences between the assays performed. C2C12 cells were culture on PLLA or PLLA/ZnO for 4 d with differentiation media or C2C12 cells were culture on PLLA or PLLA/ZnO for 14 d with growth media. **(b)** Representative images of sarcomeric myosin immunostaining (green) and DAPI (red) are presented at 4 d with differentiation media (scale bar: 200 μm) and **(c)** percentage of differentiation was calculated at 4 d as number of cells differentiated per total number of cells. **(d)** C2C12 proliferation curves (cells/cm^2) during 2 weeks of culture in

growth medium. **(e)** Representative images for sarcomeric myosin and DAPI at 14 d of culture with growth media (scale bar: 100 μm) and **(f)** percentage of differentiation was calculated at 14 d. **(g)** Fusion index distribution (number of nuclei per myotube) at 14 d was calculated and **(h)** myotube thickness distribution (μm) at 14 d is also shown. Statistical significance was observed in a t-test (***) p-value < 0.001.

Tables

Table 1. Hydrolytic degradation parameters for neat PLLA and PLLA/ZnO 1wt.% nanocomposite upon degradation in distilled water. Thermal properties (X_c crystallinity degree, T_{cc} cold crystallization temperature and T_m melting temperature), pH values of the degradation medium, water absorption (WA) and remaining weight (RW) (mean ± SD).

	0 days		**8 days**		**15 days**	
	PLLA	**PLLA/ZnO**	**PLLA**	**PLLA/ZnO**	**PLLA**	**PLLA/ZnO**
X_c **(%)**	12±1	13±1	16±2	38±1	19±2	47±3
T_{cc} **(ºC)**	102.5±0.9	95.3±1.2	93.1±0.1	79.5±0.5	91.3±1.0	78.1±0.5
T_m **(ºC)**	174.2±1.0	173.9±0.8	175.8±0.8	171.9±0.9	176.0±0.7	171.1±0.3
pH	7.40±0.10	7.40±0.10	7.37±0.08	7.36±0.10	7.29±0.12	7.18±0.13
RW (%)	100	100	99.4±0.7	99.1±0.8	98.6±0.5	98.1±0.8
WA (%)	0	0	2.3±0.9	9.6±2.1	4.7±0.9	29.4±3.2

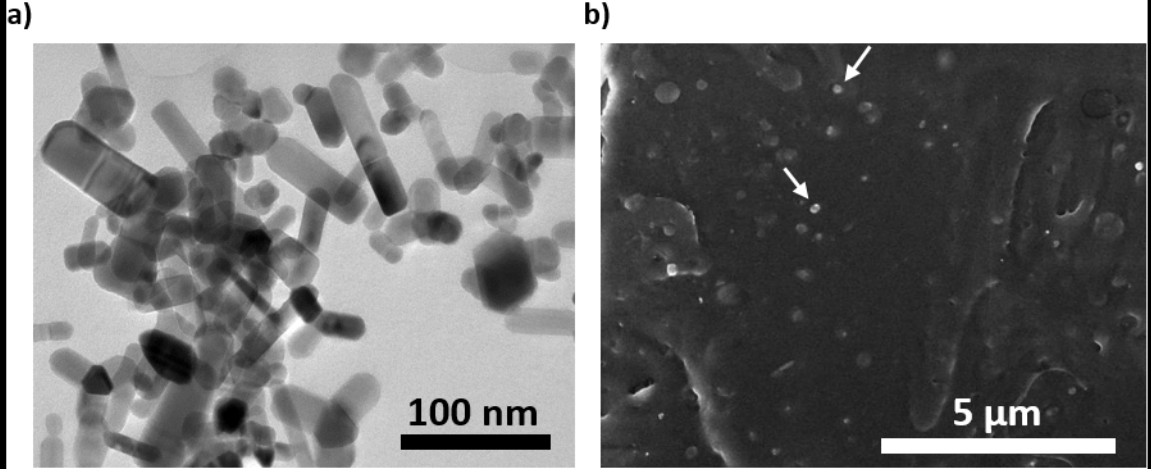
a)
100 nm
b)
5 µm

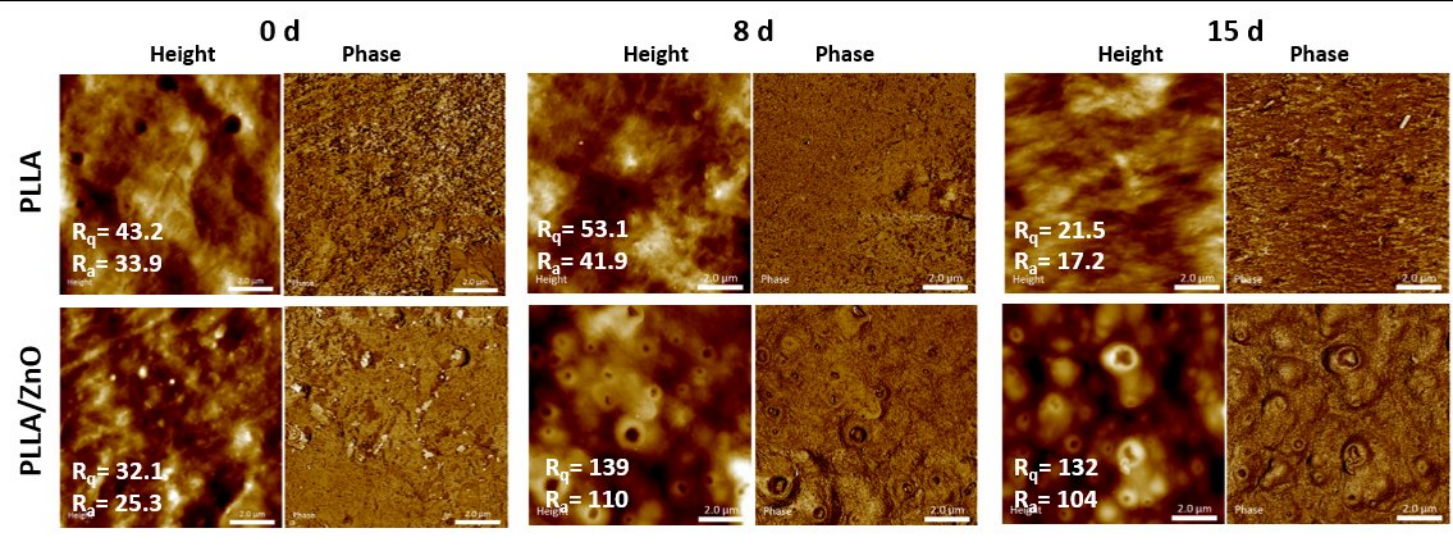
0 d
8 d
15 d
Height
Phase
Height
Phase
Height
Phase
PLLA
PLLA/ZnO
R_q= 43.2
R_a= 33.9
R_q= 53.1
R_a= 41.9
R_q= 21.5
R_a= 17.2
R_q= 32.1
R_a= 25.3
R_q= 139
R_a= 110
R_q= 132
R_a= 104
2.0 µm
Height
Phase

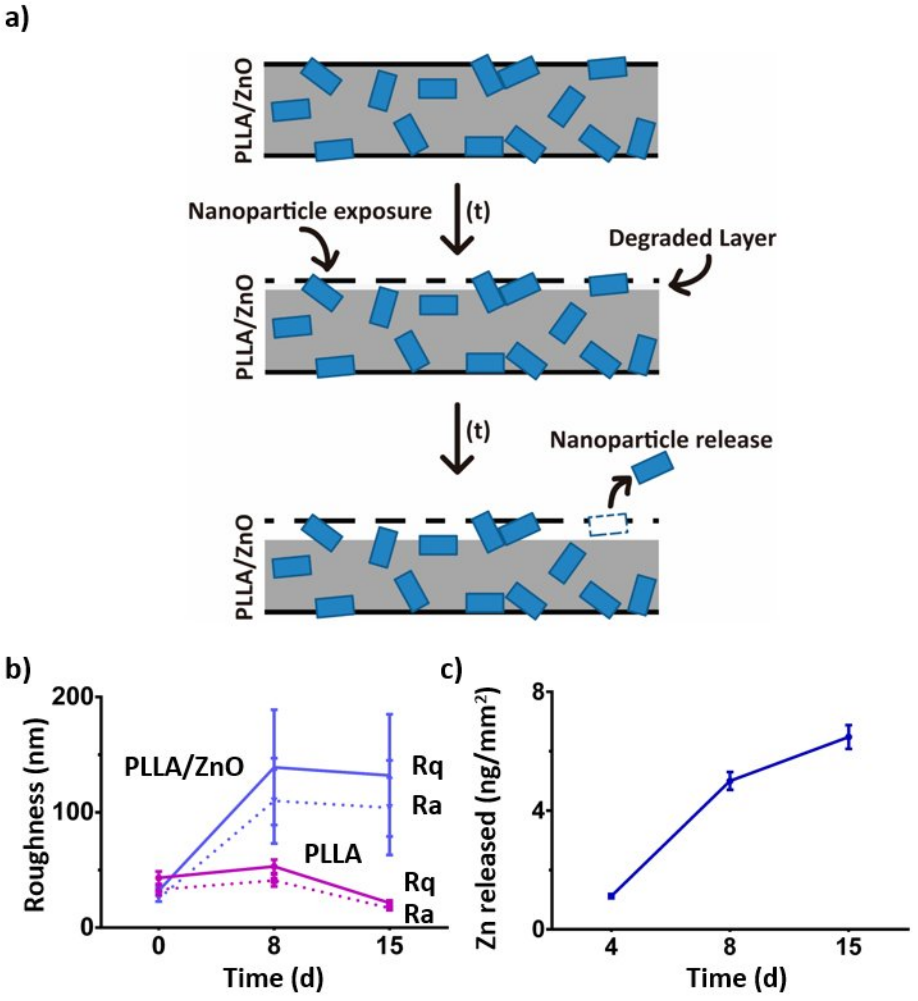
a)
PLLA/ZnO
Nanoparticle exposure
(t)
Degraded Layer
PLLA/ZnO
(t)
Nanoparticle release
PLLA/ZnO
b)
Roughness (nm)
200
100
0
PLLA/ZnO
Rq
Ra
PLLA
Rq
Ra
0
8
15
Time (d)
c)
Zn released (ng/mm²)
8
4
0
4
8
15
Time (d)

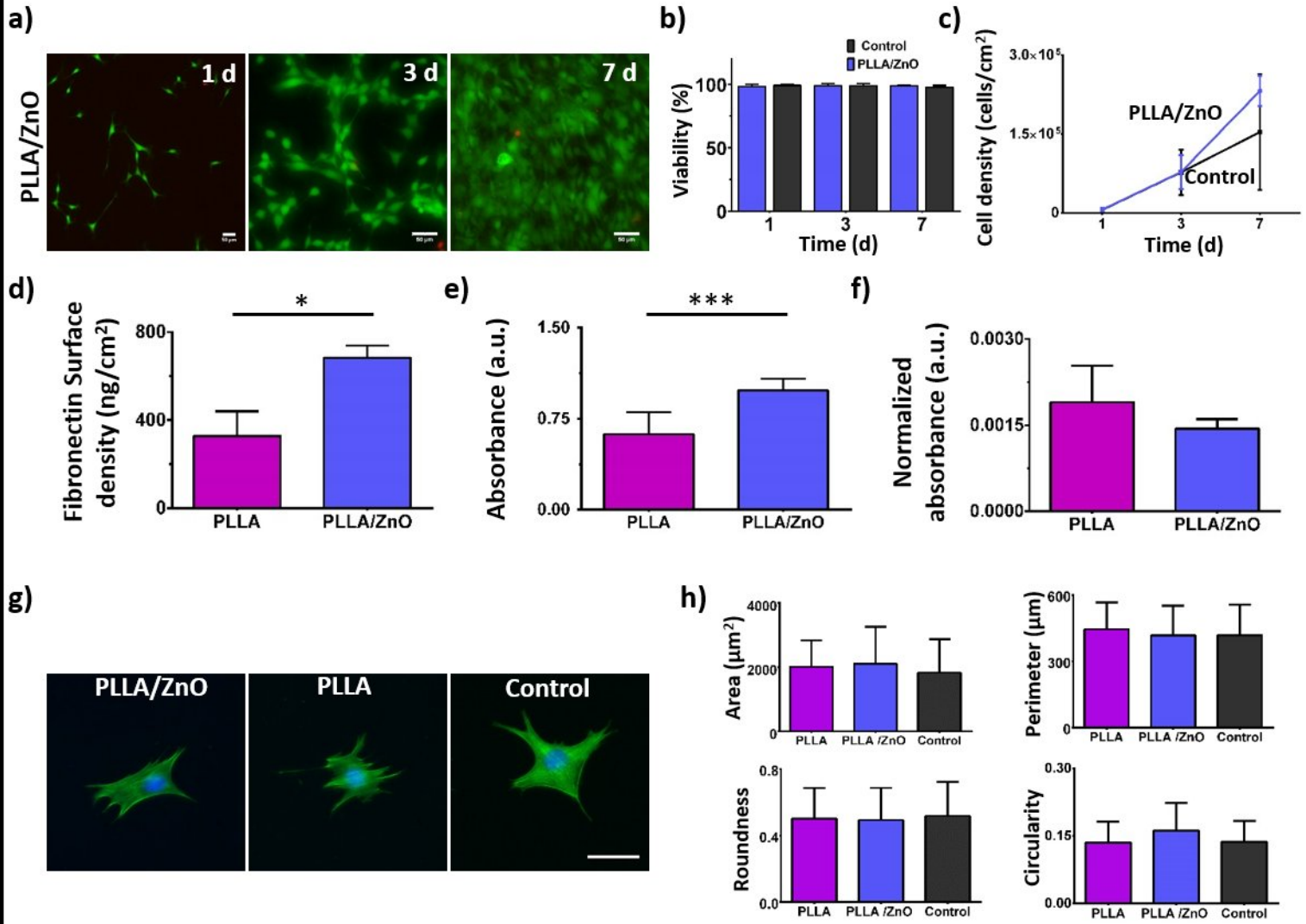
a)
PLLA/ZnO
1 d
3 d
7 d
b)
Control
PLLA/ZnO
Viability (%)
100
50
0
1
3
7
Time (d)
c)
Cell density (cells/cm²)
3.0×10⁵
1.5×10⁵
0
PLLA/ZnO
Control
1
3
7
Time (d)
d)
Fibronectin Surface density (ng/cm²)
*
800
400
0
PLLA
PLLA/ZnO
e)
Absorbance (a.u.)
***
1.50
0.75
0.00
PLLA
PLLA/ZnO
f)
Normalized absorbance (a.u.)
0.0030
0.0015
0.0000
PLLA
PLLA/ZnO
g)
PLLA/ZnO
PLLA
Control
h)
Area (μm²)
4000
2000
0
PLLA
PLLA /ZnO
Control
Perimeter (μm)
600
300
0
PLLA
PLLA /ZnO
Control
Roundness
0.8
0.4
0.0
PLLA
PLLA /ZnO
Control
Circularity
0.30
0.15
0.00
PLLA
PLLA /ZnO
Control

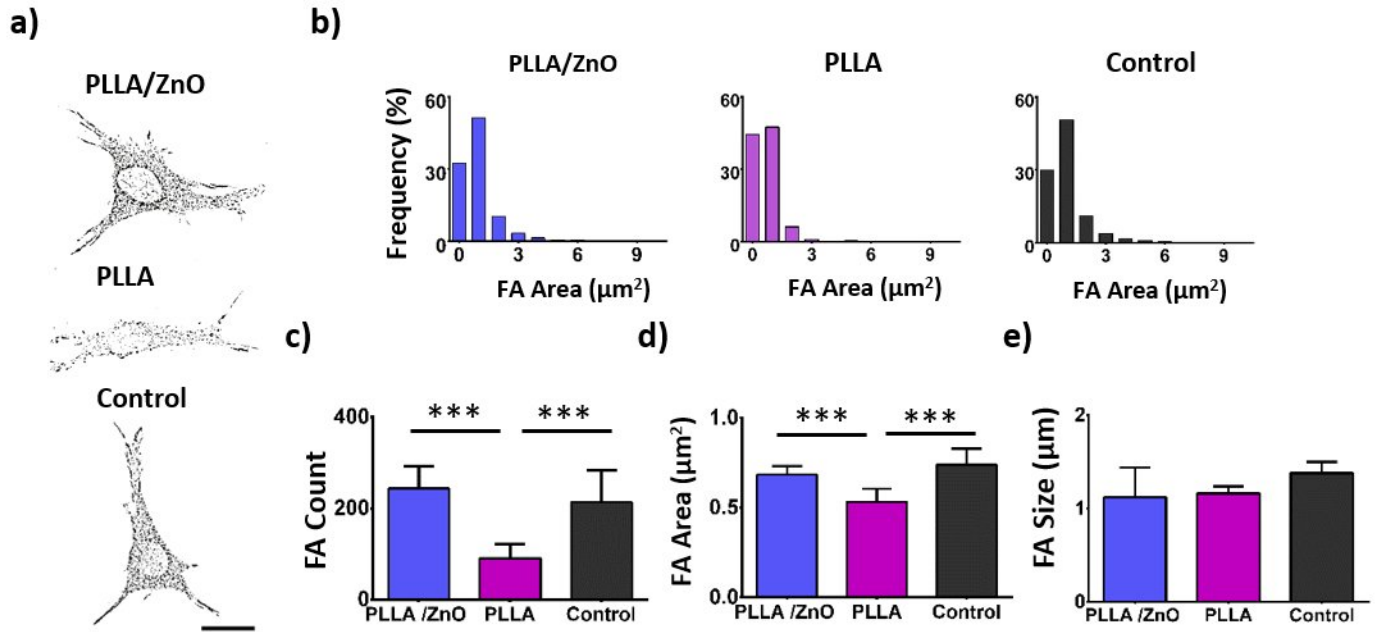
a)
PLLA/ZnO
PLLA
Control
b)
PLLA/ZnO
PLLA
Control
Frequency (%)
60
30
0
0
3
6
9
FA Area (μm²)
c)
FA Count
400
200
0
***
***
PLLA /ZnO
PLLA
Control
d)
FA Area (μm²)
1.0
0.5
0.0
***
***
PLLA /ZnO
PLLA
Control
e)
FA Size (μm)
2
1
0
PLLA /ZnO
PLLA
Control

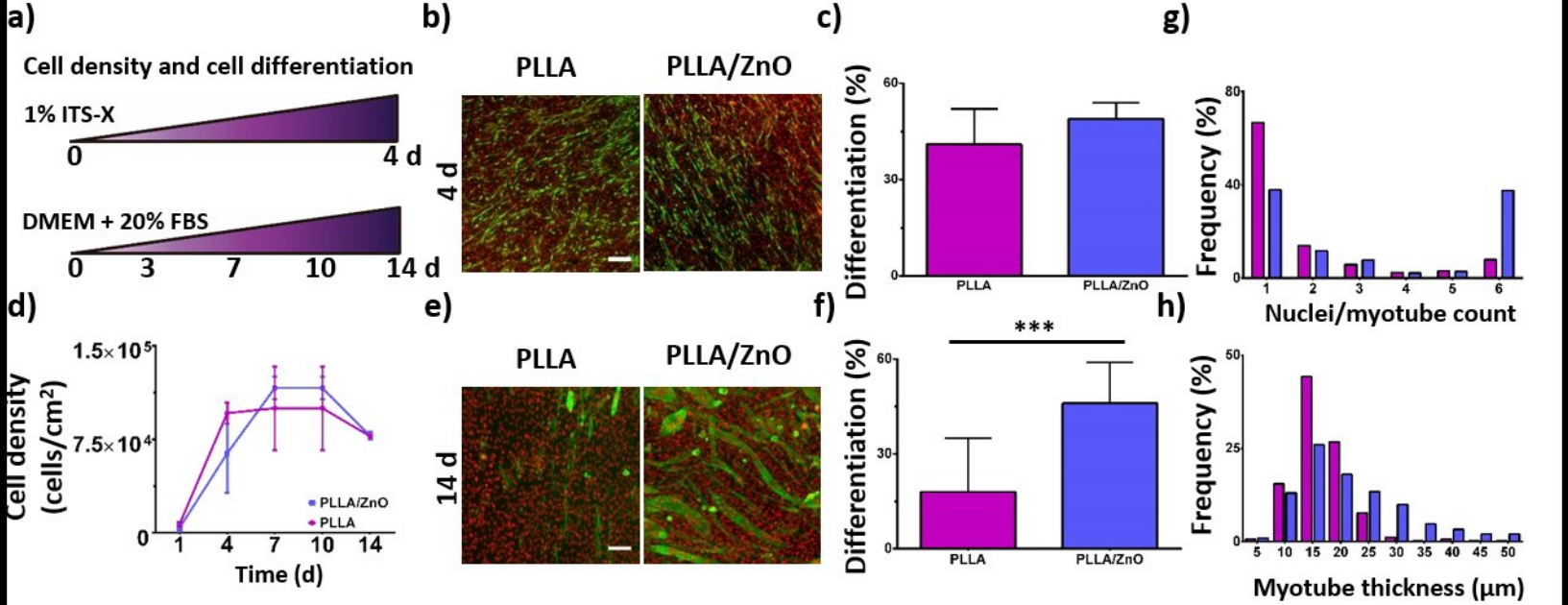
a)
Cell density and cell differentiation
1% ITS-X
0
4 d
DMEM + 20% FBS
0
3
7
10
14 d
b)
PLLA
PLLA/ZnO
4 d
c)
Differentiation (%)
60
30
0
PLLA
PLLA/ZnO
g)
Frequency (%)
80
40
1
2
3
4
5
6
Nuclei/myotube count
d)
Cell density (cells/cm²)
1.5×10⁵
7.5×10⁴
0
PLLA/ZnO
PLLA
1
4
7
10
14
Time (d)
e)
PLLA
PLLA/ZnO
14 d
f)
***
Differentiation (%)
60
30
0
PLLA
PLLA/ZnO
h)
Frequency (%)
50
25
0
5
10
15
20
25
30
35
40
45
50
Myotube thickness (μm)